Adsorptive Removal of As(V) from Aqueous Solution onto Steel Slag Recovered Iron – Chitosan Composite: Response Surface Modeling and Kinetics

Vijayanand Nagarajan[1]*, Raja Ganesan[1], Srinivasan Govindan[2], Prabha Govindaraj[3]

[1] Department of Chemistry, Paavai Engineering College (Autonomous), Anna University, NH-44 Paavai Nagar, 637 018 Namakkal, Tamil Nadu, India
[2] Department of Chemical Engineering, Paavai Engineering College (Autonomous), Anna University, NH-44 Paavai Nagar, 637 018 Namakkal, Tamil Nadu, India
[3] Department of Applied Science and Technology, Alagappa College of Technology, Anna University, Kotturpuram, 600025 Chennai, Tamil Nadu, India
* Corresponding author, e-mail: vijayanandnagarajanpec@paavai.edu.in

Abstract

In the present work iron particles was recovered by dry magnetic separation, from waste steel slag, doped with chitosan for adsorbent prepared, characterized and evaluated for the removal of As(V) from an aqueous solution. The adsorption of As(V) was optimized by using response surface methodology through Box-Behnken design model, which gave high correlation coefficient (R^2 = 0.9175), and a predictive model of quadratic polynomial equation. Analysis of variance and Fischer's F-test were used to govern the parameters which interrupt the adsorption of As(V).The adsorbent was characterized by FTIR, XRD and SEM. Optimal conditions, including adsorbent dosage, pH, temperature, initial ion concentration and contact time for the removal of As(V), were found to be 0.8 g, pH 4, 308 K, 10 mg L^{-1} and 3 h, respectively. Langmuir isotherm model fitted better compared to the Freundlich model having a maximum adsorption capacity of 11.76 mg g^{-1}, a high regression coefficient value of 0.993 and least chi-square value of 0.1959. The process was found to follow monolayer adsorption and pseudo-second-order kinetics. Thermodynamic parameters such as ΔS, ΔH and ΔG indicated the feasibility, spontaneous and endothermic nature of adsorption. Successful regeneration of the adsorbent implies its applicability to the removal of arsenic from real life wastewater.

Keywords

arsenic, steel slag, chitosan, thermodynamic, response surface methodology

1 Introduction

Arsenic is a pervasive element in the environment and has been known as a notorious toxic substance to man and living organisms for centuries [1]. Groundwater arsenic is primarily associated with oxidative weathering and geochemical reactions. Carbon plays a major role in the mobilization of arsenic in the sediments [2]. Over 100 million people in Bangladesh, West Bengal, China, Mexico, Chile, Myanmar, and United states [3] were affected by the arsenic contaminated water. Long term exposure to arsenic in drinking water causes skin diseases (pigmentation, dermal hyperkeratosis, and skin cancer), cardiovascular, neurological, liver, kidney, and prostate cancers [4]. To protect public health, the World Health Organization has set a provisional guideline limit of 10 μg L^{-1} for arsenic [5] in drinking water. The removal of arsenic by various methods has been widely reviewed [6]. Co-precipitation, flotation, ion-exchange, ultra-filtration, and reverse osmosis have been received more attention due to its high concentration efficiency. Several adsorbents have been found suitable for arsenic removal counting activated carbon [7], activated alumina [8], red mud [9], etc. In the last decade developments in the knowledge of biosorption exposed high adsorption capacities, low costs and regenerability of natural biosorption materials [10]. However, challenges encountered for biosorbents with high uptake, low cost and as well as in understanding the mechanism of biosorption with heavy metals. Chitin, a major component of crustacean shell and fungal biomass, on N-deacetylation produced chitosan. Chitin availed enormously from seafood

processing wastes. Chitosan has been found to have good sorption capacity for many heavy metal ions, owing to its high amino content [11], through complexation with the amine groups present. The fact of a high attractiveness exist between inorganic arsenic species and iron advanced to develop Fe (III) bearing materials like goethite and hematite [12], ferrihydrite [13], and iron-doped activated carbons [14] for arsenic adsorption. Studies also recognized the applicability of chitosan-Fe nanoparticles for the removal of hexavalent chromium. Therefore, iron-doped chitosan nanoparticles should be a capable biosorbent for removing heavy metals, due to the presence of the amine and hydroxyl groups. In this study, a novel iron doped chitosan composite was prepared through a simple co-precipitation method, their performance was characterized and the sorption, isotherms, kinetics and thermodynamic property for removing arsenic from aqueous solution were investigated.

2 Materials and methods
2.1 Materials
Samples of desulfurized (De-S) fresh slag fines are collected from Steel Authority of India Limited (SAIL) Salem steel plant, chemical compositions of these slag fines are presented in Table 1. Chitosan (CS, MW = 2.65×10^5 Da) with > 80 % deacetylation degree, Sodium hydrogen arsenate ($Na_2HAsO_4.7H_2O$), Sodium hydroxide and acetic acid were of analytical grade, acquired from Sigma Aldrich. Stock As(V) solution (1000 mg L^{-1}) was prepared from sodium hydrogen arsenate. All the reagents and glassware were prepared and rinsed with double de-ionized water.

2.2 Magnetic separation of iron with a pilot magnetic
2.2.1 Drum separator
Slag fines of < 10 mm size have been grinded by Soft Grinding (SG) methods for 30 min to recover fine particles of < 1 mm size. The SG mode has an advantage, over Classic Ball Grinding (CBG), by avoiding overproduction of fine particles which hamper the effectiveness of physical dry separation techniques. Dry magnetic drum separator, in Fig. 1, illustrates its working principle [15], which has a fixed permanent magnet cluster, a revolving nonmagnetic shell, and a splitter underneath the drum. On feeding the steelmaking slag particles into separator, the revolving shell brings the slag fines towards the drum bottom. More-magnetic particles gathered on the surface of the shell and fall onto the more magnetic product pile, while less-magnetic particles are thrown away from the drum surface and fall onto the less-magnetic product split. The separation can be further tuned by changing the splitter positions either towards drum surface for higher iron grade or away from the drum for higher yield of the more-magnetic product. The operating features of the drum are rotation at a constant speed of 36 rpm, field strength of 1650 gauss, drum radius of 400 mm, drum flesh thickness of 2 mm and splitter gap of 25 to 35 mm. The pilot magnetic drum separator used in this experimental work has the full features of an industrial magnetic drum separator [16].

2.3 Preparation of iron doped chitosan composite
Briefly, the synthesis procedure is as follows, the FeO particles (0.15 g) were dispersed in 2 % (v/v) acetic acid

Table 1 Chemical compositions of raw steel making slag fines (dry basis), wt%

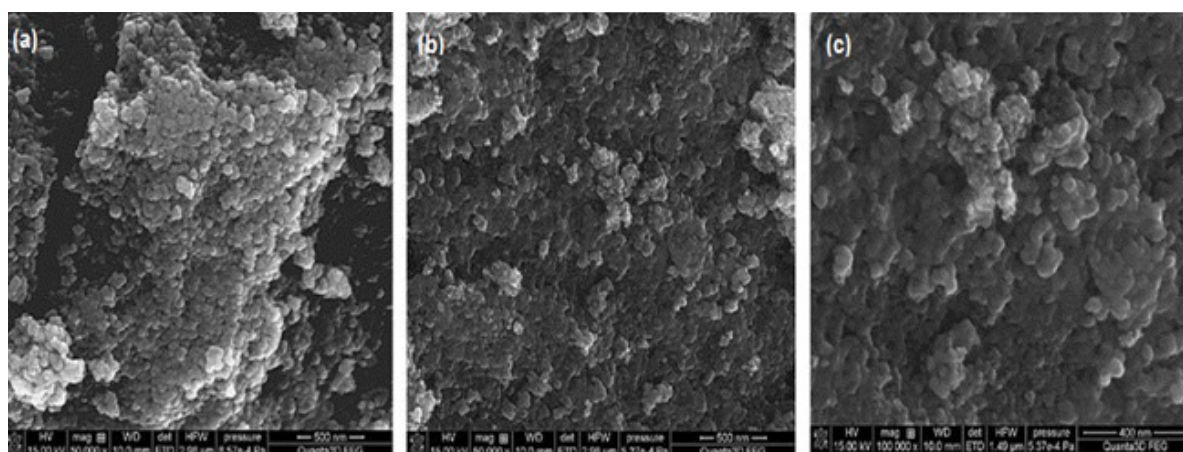| Slag type	Sample	MFe	TFe	SiO_2	Al_2O_3	CaO	MgO	MnO	P	Cr_2O_3	C	S
De-S	De-S1	12.34	34.51	9.19	2.16	29.86	5.21	1.89	0.18	0.14	3.32	0.561
	De-S2	15.21	36.48	9.16	2.31	25.56	5.41	1.15	0.12	0.11	3.56	0.527

Fig. 1 SEM images of (a) pure chitosan (b) before As(V) adsorption (c) after As(V) adsorption of composite

solution (100 mL). The chitosan (1 g) was then added, and the mixture was agitated for 60 min, to reduce the agglomeration, followed by stirring. The subsequent precipitate obtained by adding 1M NaOH, was heated at 75 °C for 4 h, filtered, washed with deionized water, and finally dried in a vacuum oven at 40 °C.

2.4 Batch adsorption experiments

Batch experiments were carried out in 100 mL polyethylene bottles with 50 mL of As solution having an initial concentration of 10 mg L^{-1}. The investigation carries the effect of various parameters such as temperature (293 K – 313 K), pH (2–10), reaction time (5 min – 5 h), and adsorbent dosage (0.1 – 2 g/50 ml) in order to find the maximum uptake of arsenic ions. Samples were collected at fixed intervals and the adsorbent was removed by centrifugation at 6000 rpm for 6 min. The supernatant was analyzed for As(V) removal by AAS. Blanks were used for control in all the experiments. The amount of arsenic adsorbed (mg g^{-1}) was determined by using the Eq. (1):

$$q_e = (C_o - C_e) \times v/m, \qquad (1)$$

where C_o and C_e are the initial and equilibrium concentrations of the metal ion (mg L^{-1}), m is the dry mass of iron-doped chitosan (g) and v is the volume of the solution (L). The % removal of As(V) from aqueous solution was calculated by using Eq. (2):

$$\text{Removal}(\%) = \left[(C_o - C_e)/C_o\right] \times 100. \qquad (2)$$

2.5 Design of experiments

The adsorption of As(V) process using the composite was demonstrated and optimized by a Box-Behnken Method (BBM) experimental design in RSM. For data analysis, design expert software (Stat Ease, Inc., Trial version 11, USA) was used. Batch experiments were performed based on BBM to investigate the effect of all four parameters. Equation (3) explains the coded values of the process variables:

$$X_i = \frac{(x_i - x_{oi})}{\Delta x_i}, \quad i = 1, 2, 3 \ldots \ldots k, \qquad (3)$$

where X_i and x_i are the coded and uncoded values of the ith variables, x_{oi} denotes the uncoded values of the ith variable at the center point, and Δx_i is the step change value. The levels of various parameters used in BBM design are represented in Table 2.

Table 2 Factors and level of various parameters of BBM design for As(V) adsorption

| Variables | Code | Level of factors | | |
		−1	0	1
Temperature (K)	x_1	303	308	313
pH	x_2	3	4	5
Contact time (min)	x_3	120	180	240
Adsorbent dosage(mg L^{-1})	x_4	600	700	800

The % removal of As(V) was determined by the following second order polynomial equation (Eq. (4)):

$$Y = \beta_0 + \sum_{i=0}^{4} \beta_i x_i + \sum_{i=0}^{4} \beta_{ii} x_i^2 + \sum_{i,j=1(i \neq j)}^{4} \beta_{ij} x_i x_j + \varepsilon, \qquad (4)$$

where Y is the response variable, β_o, β_i, β_{ij} and β_{ii} are the regression coefficients for intercept, linear effect, double interaction, and quadratic effects, respectively, x_i, x_j are the independent variables, and ε is a random error. Statistical analysis system and Tera plot software were used for the study of Analysis of variance (ANOVA), response surface studies and 3D surface plot generation respectively.

2.6 Analytical measurements

Fourier transform infrared spectra (FT-IR) and SEM analysis of the adsorbent recorded before and after As(V) adsorption with KBr discs in the range of 500–4000 cm^{-1} by Jasco-4200 and JOEL JSM-6360 scanning electron microscope at 15 kv respectively. A Shimadzu AA 7000 model Atomic Absorption Spectrometer (AAS) was used to measure the concentration of adsorbed arsenic at 194 nm with an air-acetylene flame type.

3 Results and discussion
3.1 Instrumental analysis

Morphology study, (Fig. 1 (a), (b) and (c)), shows that the adsorbent is porous in nature and entitles good complexes with adsorbed arsenic ions. XRD diffraction peaks in Fig. 2 (a), of the composite, are found consistent with the standard XRD pattern of cubic FeO (JCPDS, no.65-3107) with Fig. 2 (b).The IR spectrum peak at 3450 cm^{-1} of pure chitosan (Fig. 2 (a) confirms the primary alcoholic group [17], and peak at 588 cm^{-1} (Fig. 2 (b)) of Fe-O group [18] presence. After As(V) adsorption (Fig. 2 (c)), the peak shift from 1655 to 1642 cm^{-1}, new bands at 1560 cm^{-1} and 834 cm^{-1} predicts the amine dislodgement [19], nitrogen atom responsibility, and the existence of As(V) [20] in the adsorbent respectively.
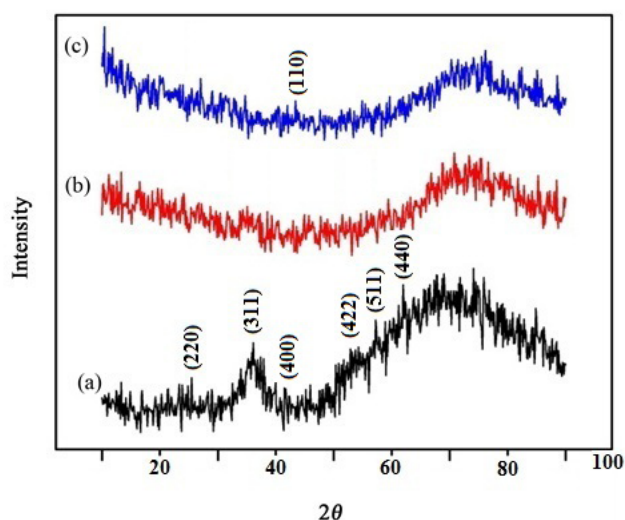
Fig. 2 XRD patterns of (a) FeO-Chitosan composite (b) FeO only
(c) As(V) adsorbed FeO-Chitosan composite

3.2 Quadratic model for As(V) adsorption

The adsorbent As(V) removal capacity was optimized by employing the BBM technique. Table 3, display the 29 runs of experimental designs, along with corresponding adsorption results. The removal efficiency as functions of temperature (x_1), pH (x_2), reaction time (x_3) and adsorbent dosage (x_4) was correlated with the developed second-order polynomial equation given in Eq. (5):

$$\% \text{ removal of As}(V) = -276.05000 + 13.506677x_1$$
$$+ 11.55000x_2 + 8.6667x_3 + 0.213333x_4 + 0.190000x_1x_2$$
$$- 0.090000x_1x_3 - 0.003150x_1x_4 + 0.450000x_2x_3$$
$$+ 0.005000x_2x_4 - 0.000250x_3x_4 - 0.159167x_1^2$$
$$- 2.79167x_2^2 - 1.15417x_3^2 - 0.000074x_4^2.$$

$$(5)$$

The effect of independent variables on the adsorption efficiency of As(V) was described by the above equation predicts a maximum As(V) removal of 92 %.

Experimental curve fitting was evaluated to govern the significant model for this system (Table 4). Each type of model was calculated for Fischer F-test value. In general, larger F- and lower probability values (p-values) with significant terms were chosen. From the data given in Table 4, a quadratic model was suggested for higher F-value (23.49) and lower p-value (< 0.0001) with significant terms for this experimental design on compared with other models. The cubic model was found to be insignificant.

ANOVA justifies the significance of the quadratic model by correlating the model with the response variables. Table 5, shows the variables denoted in ANOVA was the main effects, the interaction effects, and the error terms.

Table 3 Experimental design with adsorption results

Std	Run	A: x_1 (k)	B: x_2	C: x_3 (h)	D: x_4 (mg L^{-1})	Removal of As(V)%
			Coded levels			
4	1	313	5	3	800	89.7
16	2	308	5	4	800	90.1
8	3	308	4	4	900	89.8
12	4	313	4	3	900	88.8
27	5	308	4	3	700	91.3
23	6	308	3	3	900	85.5
7	7	308	4	2	900	91.1
9	8	303	4	3	700	82.9
6	9	308	4	4	700	89.6
13	10	308	3	2	800	87.2
21	11	308	3	3	700	86.1
15	12	308	3	4	800	88.3
24	13	308	5	3	900	89.9
19	14	303	4	4	800	85.5
1	15	303	3	3	800	83.1
17	16	303	4	2	800	84.2
22	17	308	5	3	700	88.5
26	18	308	4	3	800	91.8
11	19	303	4	3	900	87.6
18	20	313	4	2	800	87.2
5	21	308	4	2	700	90.8
25	22	308	3	3	800	90.8
14	23	308	5	2	800	87.2
28	24	308	4	4	800	91.4
29	25	308	4	3	900	91.6
10	26	313	4	3	700	90.4
20	27	313	4	4	800	86.7
3	28	300	5	3	800	84.2
2	29	313	3	3	800	84.8

Table 4 Experimental curve fitting of optimization

Source	Sum of Squares	DF	Mean Square	F-	p-value Prob $> F$	Remarks
Linear vs mean	53.49	4	13.3	1.92	0.140	-
2FI vs linear	16.16	6	2.69	0.32	0.917	-
Quadratic vs 2FI	131.55	4	32.8	23.4	< 0.0001	Suggested
Cubic vs quadratic	12.52	8	1.57	1.33	0.3752	Aliased

The importance of these variables was represented by F and p values. In the quadratic model developed, the F-value of 10.26 indicated that the model was statistically significant and there is only a 0.01 % chance that an F-value this large

Table 5 Analysis of variance for the quadratic model by BBM optimization for As(V) adsorption

Source	Sum of Squares	DF	Mean Square	F-value	p-value Prob $> F$	Remarks
Model	201.19	14	14.37	10.26	< 0.0001	Sig*
x_1 (k)	33.67	1	33.67	24.05	0.0002	Sig*
x_2	17.76	1	17.76	12.69	0.0031	Sig*
x_3 (min)	0.4408	1	0.4408	0.3149	0.5836	-
x_4 (mg L^{-1})	1.61	1	1.61	1.15	0.3012	-
$x_1 x_2$	3.61	1	3.61	2.58	0.1306	-
$x_1 x_3$	0.8100	1	0.8100	0.5785	0.4595	-
$x_1 x_4$	9.92	1	9.92	7.09	0.0186	Sig*
$x_2 x_3$	0.8100	1	0.8100	0.5785	0.4595	-
$x_2 x_4$	1.0000	1	1.0000	0.7143	0.4122	-
$x_3 x_4$	0.0025	1	0.0025	0.0018	0.9669	-
x_1^2	102.71	1	102.71	73.36	< 0.0001	Sig*
x_2^2	50.55	1	50.55	36.11	< 0.0001	Sig*
x_3^2	8.64	1	8.64	6.17	0.0263	Sig*
x_4^2	3.57	1	3.57	2.55	0.1327	-
Residual	19.60	14	1.40	-	-	-
Lack of fit	19.60	10	1.96	-	-	Not Sig#
Pure error	0.0000	4	0.0000	-	-	-
Cor total	220.79	28	-	-	-	-

* Significant   # Not Significant

could occur due to noise. The model suggested was highly significant due to its p-value of < 0.0001. The Table 5 shows the six significant terms with low p-values were x_1, x_2, $x_1 x_4$, x_1^2, x_2^2 and x_3^2. Other significant terms were not discussed because of their high p-values. The above model accuracy could be assessed by the fortitude of regression coefficient R^2. The value of $R^2 = 0.9112$, in the present study, indicated that only 9 % of the total variables were not explained by the model. The adjusted coefficient value (R^2 adj $= 0.8225$) was not in realistic arrangement with observed R^2. The model has undesirable lack of fit by the indication of lack of fit p-value (> 0.05) suggested that it is not significantly relative to the pure error and, thus, above quadratic equation and the model were accurate for the experiment [21]. The value of signal to noise ratio was found to be 10.238, ratio > 4 is desirable, indicated an adequate signal to navigate the design space. The Fig. 3, of the graph, plotted between actual and predicted values for removal of As(V), indicated that the distribution of actual values were relatively close to the straight line which, specifies the quadratic model was necessary for predicting the efficient removal of As(V) under the parameters studied.
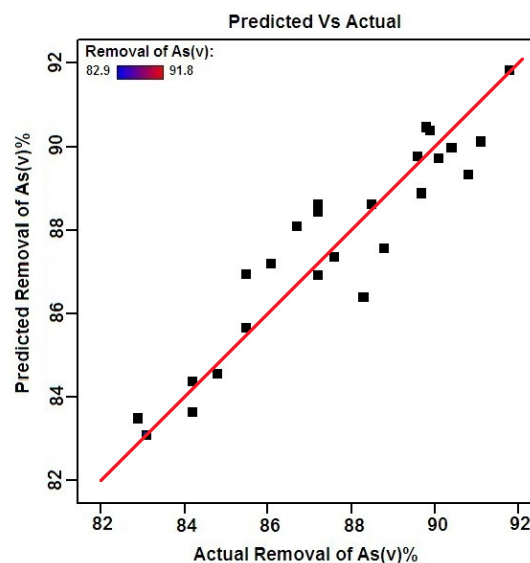
Fig. 3 Comparison between actual and predicted values of RSM model on optimized parameters for As(V) removal

The plot between studentized residuals and run number, in Fig. 4, showed that the random distribution of residuals around ±3.9 (limit is $< ±4.00$) [21] was a good sign of well fitted experimental data with the model.

3.3 Effect of process variables on removal of As(V)

To optimize the process variables of equilibrium conditions, from batch experiments, it was necessary to study the impact of each variable on the adsorption process. Hence, three-dimensional curves were plotted between the variables of temperature, pH, reaction time and adsorbent dosage. Fig. 5 (a), represents the effect of temperature and pH indicated that
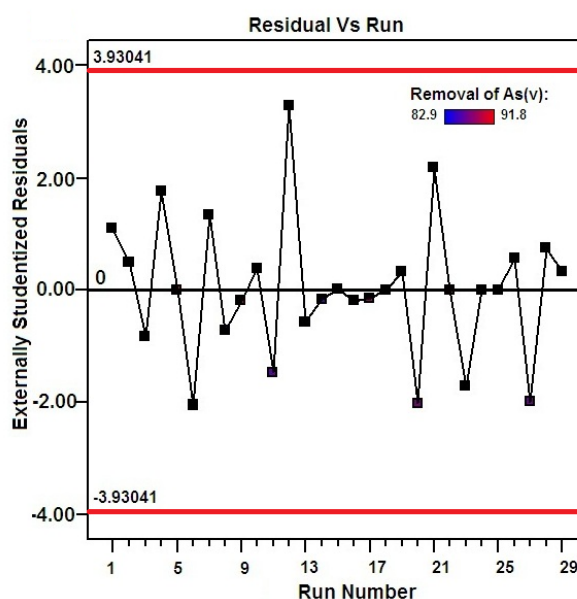
Fig. 4 Plot of studentized residuals versus experimental run number on optimized parameters for As(V) removal.
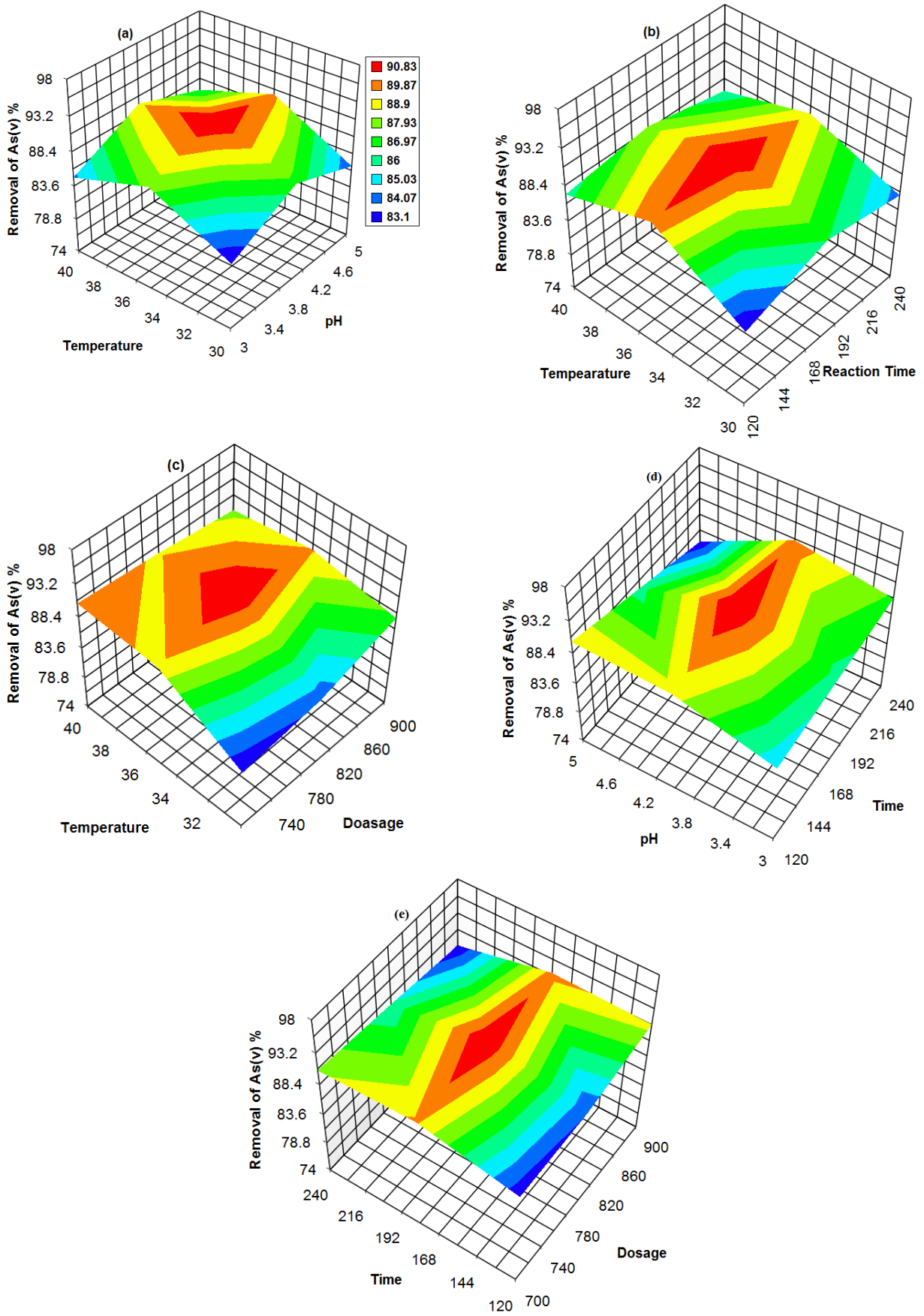
Fig. 5 3D surface mapping plot for multiple effects of (a) temperature and pH (b) temperature and time (c) dosage and temperature (d) time and pH (e) reaction time and adsorbent dosage on As(V) removal.

the adsorption reaches maximum at 308 K on pH 4 and then decreases, infers that the process is dependent on pH and temperature. It may due to desorption, at higher pH and temperature, the decreasing trend in adsorption continues.

The correlation of temperature and reaction time is as shown in Fig. 5 (b). The optimal adsorption efficiency of 91.8 % was reached within 180 min at temperature of 308 K. The observation found that as contact time (> 180 min) and temperature (> 35 °C) increased, the adsorption rate decreased.

The plot of temperature versus adsorbent dosage in Fig. 5 (c), shows that the degree of adsorption increases with increasing adsorbent dosage, up to 800 mg on 308 K, due to high surface availability. While beyond 800 mg dosage and 308 K it has equilibrium and decreasing trend starts for the variables respectively infer, that the temperature plays a major role in the adsorption procedure.

Fig. 5 (d) shows the effect of time and pH. The adsorption capacity was almost constant with respect to time in the pH range 3–3.7. When the pH was beyond 3.7 the adsorption increases and reaches maximum at pH 4. The relation of reaction time and adsorption dosage plotted in Fig. 5 (e), fairly indicates that the adsorption rate is almost constant on increasing time and gradually increases with respect to dosage and reaches maximum adsorption level at 180 min and 800 mg respectively.

From the above, process variable correlations studied, it was evident that the adsorption rate was remarkably affected by temperature and pH, while the contact time and adsorbent dosage had fringe effect only. The above fact is supported by the contour plot, in Fig. 3, between pH and temperature which also shows that the experimental and predicted removal efficiency was 91.8 % and 92 % respectively with a difference of minimum 0.2 % under the optimal conditions. By the observation, the adsorption is endothermic in nature and takes place by diffusion and complexation process [22] respectively. The increase in the adsorption capacity was due to both the increase of the diffusion rate of As(V) and the rate of complexation with the functional groups present in the adsorbent [23].

3.4 Adsorption isotherms

The isotherm equations could be used to describe the sorption data, sorption mechanism, the surface properties and the affinity between sorbent and sorbate. The various isotherms models employed in the linear form [24], equilibrium parameters, linear regression analysis, and computed constants were shown in Table 6.

Table 6 Comparison of equilibrium parameters at different temperature

Model	Parameters	Temperature (K) 298	303	308
Langmuir	K_1 (L/mg)	10.86	10.98	11.76
	q_m (mg/g)	0.0355	0.0440	0.0573
	R^2	0.981	0.985	0.993
	R_L	0.7380	0.6944	0.6357
	RMSE	0.4999	0.4547	0.3284
	χ^2	0.3192	0.3754	0.1959
Freundlich	K_F (mg/g)	0.7298	0.7953	0.9231
	η	1.4684	1.6583	1.6694
	R^2	0.897	0.982	0.985
	RMSE	3.8007	4.3404	4.7157
	χ^2	13.827	15.64	16.8591

3.4.1 Langmuir isotherms

The linear form of the isotherm can be explained by Eq. (6) represents monolayer sorption:

$$\frac{C_e}{q_e} = \frac{1}{K_1 q_m} + \frac{C_e}{q_m}. \tag{6}$$

The maximum adsorption capacity, q_m = 10.86 − 11.76 mg g^{-1}, and higher regression coefficient, R^2 = 0.993 were obtained from the Langmuir isotherm plots (Fig. 6), suggesting that the surface was homogenous. The dimensionless factor (R_L = 1/1 + bC_o) was calculated as < 1, indicates favorable adsorption and follows monolayer process [25]. The certainty of the isotherm was committed by the least RMSE and χ^2 values than other isotherm model employed.
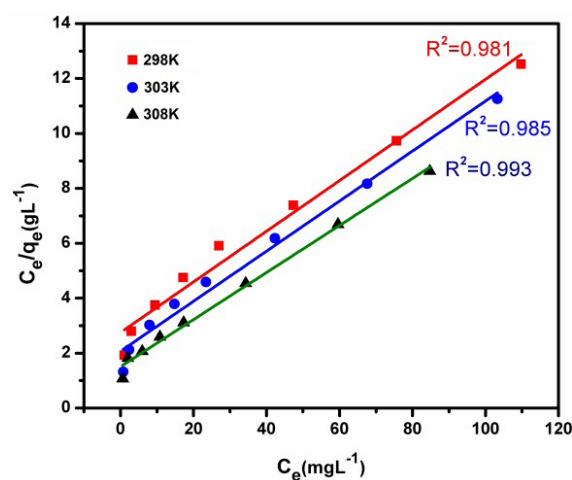

Fig. 6 Langmuir isotherm plot for the adsorption of As(V) ion by composite adsorbent. at different temperatures

3.4.2 Freundlich isotherm

The isotherm is employed by Eq. (7):

$$\log q_e = \log K_F + \frac{1}{n} \log C_e, \tag{7}$$

which describes the sorption on an energetically heterogeneous surface and the distribution of active sites and their energies [26]. The value of n (intensity) obtained, from the Freundlich model (Fig. 4), in the range 1–10 signifies the good performance of FeO doped chitosan adsorbent towards As(V) adsorption.

3.5 Residual Mean Square Error (RMSE) analysis

The R^2 values does not represent the errors in the isotherm curves. To evaluate the fit of the isotherm equations, the RMSE [27] analysis is employed.

$$\text{RMSE} = \sqrt{\frac{1}{n-2} \sum_{i=1}^{n} \left(q_{e,exp} - q_{e,cal} \right)^2} \tag{8}$$

$q_{e,exp}$, $q_{e,cal}$ and n are the experimental, calculated values and number of observations respectively. The smaller the RMSE value the better the curve fitting. From Table 7, it assures that the process best fit was affirmed for Langmuir model.

3.6 Chi-square (χ^2) statistical test

The χ^2 test confirms the suitability of a particular isotherm model [28], in describing the experimental data. Equation (9) is given as:

$$\chi^2 = \sum \frac{\left(q_{e,exp} - q_{e,cal} \right)^2}{q_{e,cal}}. \tag{9}$$

The χ^2 value would be less if the adsorption data correlated concurs with experimental values. By which, from Table 7, the adsorption suitability more correlate with the Langmuir model than other models.

3.7 Adsorption kinetics modeling

3.7.1 First order and pseudo-second-order kinetics

Kinetics study revealed the information on the solute uptake and the reaction pathways. It was evaluated using the First order and pseudo-second order equations. The pseudo-first-order linear equation elucidate mechanism of adsorption and rate controlling steps [29], explained by Eq. (10):

$$\log \left(q_e - q_t \right) = \log q_e - \frac{K_1 t}{2.303}. \tag{10}$$

However, a pseudo-second-order equation analyzed the effective adsorption capacity, initial adsorption rate and rate limiting step [30]. The linear form of pseudo-second-order equation can be represented as follows (Eq. (11)):

$$\frac{t}{q_t} = \frac{t}{k_2 q_e^2} + \frac{t}{q_e}. \tag{11}$$

The initial adsorption rate, h (mg g^{-1} min^{-1}), as $t \to 0$, can be defined by the Eq. (12):

$$h = k_2 q_e^2. \tag{12}$$

The kinetic parameters were obtained through the Pseudo first order plot (Fig. 5) and second order plot (Fig. 7), presented in Table 7.

Table 7 shows a higher regression coefficient and h values of 0.994 and 0.0878 respectively, obtained from the Pseudo second order model, exposed its applicability,
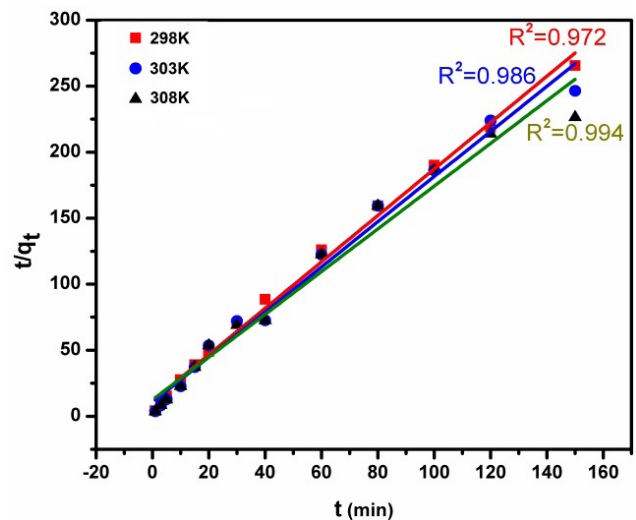

Fig. 7 Pseudo-second-order kinetics plot for the adsorption of As(V) ion at different temperatures

Table 7 Kinetic parameters of As(V) adsorption at different temperatures

Temp (K)	$q_{e,exp}$ (mg/g)	Pseudo first order				Pseudo Second order			
		$q_{e,cal}$ (mg/g)	k_2/min	R^2		h (mg/(g min))	$q_{e,cal}$ (mg/g)	k_2/min	R^2
298	0.5578	0.5359	0.0133	0.968		0.0758	0.5715	0.2326	0.972
303	0.5775	0.5467	0.0148	0.973		0.0816	0.5792	0.2432	0.986
308	0.5860	0.5575	0.1610	0.984		0.0878	0.5866	0.2549	0.994

chemisorption and rate limiting step nature of reaction [31] in the adsorption process.

3.8 Adsorption thermodynamics

The thermodynamic parameters ΔG, ΔH, and ΔS were utilized to elucidate the feasibility of adsorption [32]. The Van't Hoff plot, Fig. 8, (ln k_c, equilibrium constant, against $1/T$) relates the parameters can be explained by Eqs. (13) and (14):

$$\ln k_c = \frac{-\Delta H}{RT} + \frac{\Delta S}{R}, \tag{13}$$

$$\Delta G = -RT \ln k_c. \tag{14}$$

The calculated values of the energy parameters ΔG, ΔH, and ΔS are given in the Table 8.

The negative ΔG, free energy values, positive value of enthalpy, $\Delta H = 6.0724$ (< 80 kJ mol^{-1}) suggested the feasibility, spontaneous and endothermic process respectively [33]. The positive value of ΔS, entropy, reflects the affinity and structural changes in adsorbent and adsorbate during adsorption process [34].

4 Conclusions

In this study, a novel iron doped chitosan biosorbent was prepared, characterized, evaluated, and successfully employed for arsenic removal. The main variables optimized by Box-Behnken Design of RSM model ($R^2 = 0.9112$) were in good agreement with arsenic adsorption process. The maximum sorption capacity for As(V) was found to be 11.76 mg g^{-1} from the Langmuir isotherm and follows pseudo-second-order kinetics. Thermodynamic studies revealed the process is feasible, spontaneous, and endothermic in nature. Interfering ions had marginal effects on adsorption. Thus, it concluded the iron doped chitosan composite, from waste steel slag, would be a potential candidate for arsenic filtering units, due to its biocompatibility.

Fig. 8 Van't Hoff plot at different temperatures

Table 8 Thermodynamic parameters of As(V) adsorption at different temperatures

	Van't Hoff plot		
Temp (K)	ΔG (kJ/mol)	ΔH (kJ/mol)	ΔS (J mol^{-1} K^{-1})
298	−5.9090	6.0742	0.04018
303	−6.0862		
308	−6.3133		

References

[1] Chappell, W. R., Abernathy, C. O., Calderon, R. L. "Preface", In: Arsenic Exposure and Health Effects III: Proceedings of the Third International Conference on Arsenic Exposure and Health Effects, San Diego, CA, USA, 1999, pp. vii–viii.
https://doi.org/10.1016/b978-008043648-7/50001-7

[2] Chatterjee, S., De, S. "Adsorptive removal of arsenic from groundwater using chemically treated iron ore slime incorporated mixed matrix hollow fiber membrane", Separation and Purification Technology, 179, pp. 357–368, 2017.
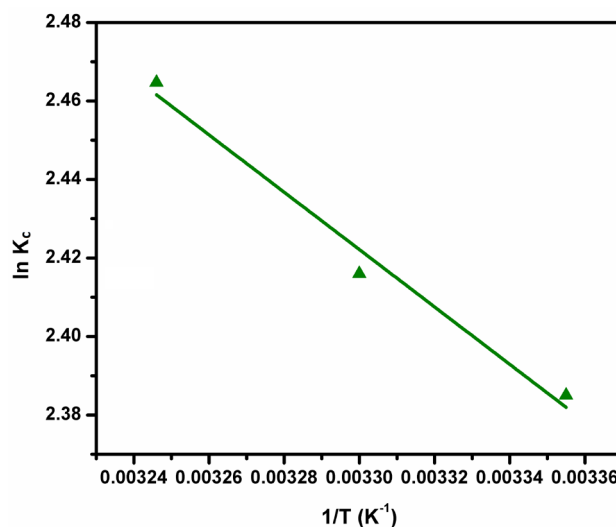https://doi.org/10.1016/j.seppur.2017.02.019

[3] Jain, C. K., Singh, R. D. "Technological options for the removal of arsenic with special reference to South East Asia", Journal of Environmental Management, 107, pp. 1–18, 2012.
https://doi.org/10.1016/j.jenvman.2012.04.016

[4] Shakoor, M. B., Nawaz, R., Hussain, F., Raza, M., Ali, S., Rizwan, M., Oh, S.-E., Ahmad, S. "Human health implications, risk assessment and remediation of As-contaminated water: A critical review", Science of the Total Environment, 601–602, pp. 756–769, 2017.
https://doi.org/10.1016/j.scitotenv.2017.05.223

[5] World Health Organization "Guidelines for Drinking-water Quality", World Health Organization (WHO), Geneva, Switzerland, 2017. [online] Available at: https://www.who.int/publications/i/item/9789241549950 [Accessed: 09 April 2019]

[6] Hao, L., Liu, M., Wang, N., Li, G. "A critical review on arsenic removal from water using iron-based adsorbents", RSC Advances, 8(69), pp. 39545–39560, 2018.
https://doi.org/10.1039/C8RA08512A

[7] Qi, J., Zhang, G., Li, H. "Efficient removal of arsenic from water using a granular adsorbent: Fe–Mn binary oxide impregnated chitosan bead", Bioresource Technology, 193, pp. 243–249, 2015.
https://doi.org/10.1016/j.biortech.2015.06.102

[8] Zhou, Z., Liu, Y., Liu, S., Liu, H., Zeng, G., Tan, X., Yang, C., Ding, Y., Yan, Z., Cai, X. "Sorption performance and mechanisms of arsenic(V) removal by magnetic gelatin-modified biochar", Chemical Engineering Journal, 314, pp. 223–231, 2017.
https://doi.org/10.1016/j.cej.2016.12.113

[9] Mahbubul Hassan, M., Davies-McConchie, J. F. "Removal of Arsenic and Heavy Metals From Potable Water by Bauxsol Immobilized onto Wool Fibers", Industrial and Engineering Chemistry Research, 51(28), pp. 9634–9641, 2012.
https://doi.org/10.1021/ie300286k

[10] Saini, A. S., Melo, J. S. "Biosorption of uranium by melanin: Kinetic, equilibrium and thermodynamic studies", Bioresource Technology, 149, pp. 155–162, 2013.
https://doi.org/10.1016/j.biortech.2013.09.034

[11] Gupta, A., Yunus, M., Sankararamakrishnan, N. "Chitosan- and Iron-Chitosan-Coated Sand Filters: A Cost-Effective Approach for Enhanced Arsenic Removal", Industrial and Engineering Chemistry Research, 52(5), pp. 2066–2072, 2013.
https://doi.org/10.1021/ie302428z

[12] Futalan, C. M., Huang, Y.-S., Chen, J.-H., Wan, M.-W. "Arsenate removal from aqueous solution using chitosan-coated bentonite, chitosan-coated kaolinite and chitosan-coated sand: parametric, isotherm and thermodynamic studies", Water Science & Technology, 78(3), pp. 676–689, 2018.
https://doi.org/10.2166/wst.2018.339

[13] Hokkanen, S., Repo, E., Lou, S., Sillanpää, M. "Removal of arsenic(V) by magnetic nanoparticles activated micro fibrillated cellulose", Chemical Engineering Journal, 260, pp. 886–894, 2015.
https://doi.org/10.1016/j.cej.2014.08.093

[14] Lunge, S., Singh, S., Sinha, A. "Magnetic iron oxide (Fe_3O_4) nanoparticles from tea waste for arsenic removal", Journal of Magnetism Magnetic Materials, 356, pp. 21–31, 2014.
https://doi.org/10.1016/j.jmmm.2013.12.008

[15] Ma, N., Houser, J. B., Wood, L. A., Lewis, R. W., Hill, D. G. "Enhancement of Iron Recovery from Steelmaking Slag Fines by Process Optimization of Upgrading the Slag Fines with Dry Magnetic Separation", Journal of Sustainable Metallurgy, 3(2), pp. 280–288, 2017.
https://doi.org/10.1007/s40831-016-0079-z

[16] Menad, N., Kanari, N., Save, M. "Recovery of high grade iron compounds from LD slag by enhanced magnetic separation techniques", International Journal of Mineral Processing, 126, pp. 1–9, 2014.
https://doi.org/10.1016/j.minpro.2013.11.001

[17] Haldorai, Y., Rengaraj, A., Ryu, T., Shin, J., Huh, Y. S., Han, Y.-K. "Response surface methodology for the optimization of lanthanum removal from an aqueous solution using a Fe_3O_4/chitosan nanocomposite", Materials Science and Engineering: B, 195, pp. 20–29, 2015.
https://doi.org/10.1016/j.mseb.2015.01.006

[18] Siddiqui, S. I., Chaudhry, S. A. "Iron oxide and its modified forms as an adsorbent for arsenic removal: A comprehensive recent advancement", Process Safety and Environmental Protection, 111, pp. 592–626, 2017.
https://doi.org/10.1016/j.psep.2017.08.009

[19] Malwal, D., Gopinath, P. "Silica Stabilized Magnetic-Chitosan Beads for Removal of Arsenic from Water", Colloid and Interface Science Communications, 19, pp. 14–19, 2017.
https://doi.org/10.1016/j.colcom.2017.06.003

[20] Kumar, A. S. K., Jiang, S.-J. "Chitosan-functionalized graphene oxide: A novel adsorbent an efficient adsorption of arsenic from aqueous solution", Journal of Environmental Chemical Engineering, 4(2), pp. 1698–1713, 2016.
https://doi.org/10.1016/j.jece.2016.02.035

[21] Sahu, U. K., Mahapatra, S. S., Patel, R. K. "Application of Box-Behnken Design in response surface methodology for adsorptive removal of arsenic from aqueous solution using CeO_2/Fe_2O_3/grapheme nanocomposite", Materials Chemistry Physics, 207, pp. 233–242, 2018.
https://doi.org/10.1016/j.matchemphys.2017.11.042

[22] Sharma, S., Bharathi, M., Rajesh, N. "Efficacy of a heterocyclic ligand anchored biopolymer adsorbent for the sequestration of palladium", Chemical Engineering Journal, 259, pp. 457–466, 2015.
https://doi.org/10.1016/j.cej.2014.08.002

[23] Chio, C.-P., Lin, M.-C., Liao, C.-M. "Low-cost farmed shrimp shells could remove arsenic from solutions kinetically", Journal of Hazardous Materials, 171(1–3), pp. 859–864, 2009.
https://doi.org/10.1016/j.jhazmat.2009.06.086

[24] Ayawei, N., Ekubo, A. T., Wankasi, D., Dikio, E. D. "Adsorption of Congo Red by Ni/Al-CO_3: Equilibrium, Thermodynamic and Kinetic Studies", Oriental Journal of Chemistry, 31(3), pp. 1307–1318, 2015.
https://doi.org/10.13005/ojc/310307

[25] Hu, Q., Liu, Y., Gu, X., Zhao, Y. "Adsorption behavior and mechanism of different arsenic species on mesoporous $MnFe_2O_4$ magnetic nanoparticles", Chemosphere, 181, pp. 328–336, 2017.
https://doi.org/10.1016/j.chemosphere.2017.04.049

[26] Jiang, Y., Gong, J.-L., Zeng, G.-M., Ou, X.-M., Chang, Y.-N., Deng, C.-H., Zhang, J., Liu, H.-Y., Huang, S.-Y. "Magnetic chitosan-graphene oxide composite for anti-microbial and dye removal applications", International Journal of Biological Macromolecules, 82, pp. 702–710, 2016.
https://doi.org/10.1016/j.ijbiomac.2015.11.021

[27] Choudhary, B., Paul, D. "Isotherms, kinetics and thermodynamics of hexavalent chromium removal using biochar", Journal of Environmental Chemical Engineering, 6(2), pp. 2335–2343, 2018.
https://doi.org/10.1016/j.jece.2018.03.028

[28] Saadi, R., Saadi, Z., Fazaeli, R., Fard, N. E. "Monolayer and multilayer adsorption isotherm models for sorption from aqueous media", Korean Journal of Chemical Engineering, 32(5), pp. 787–799, 2015.
https://doi.org/10.1007/s11814-015-0053-7

[29] Poinern, G. E. J., Parsonage, D., Issa, T. B., Ghosh, M. K., Paling, E., Singh, P. "Preparation, characterization and As(V) adsorption behavior of CNT-ferrihydrite composites", International Journal of Engineering, Science and Technology, 2(8), pp. 13–24, 2010.
https://doi.org/10.4314/ijest.v2i8.63776

[30] Kumar, A. S. K., Kumar, C. U., Rajesh, V., Rajesh, N. "Microwave assisted preparation of n-butylacrylate grafted chitosan and its application for Cr(VI) adsorption", International Journal of Biological Macromolecules, 66, pp. 135–143, 2014.
https://doi.org/10.1016/j.ijbiomac.2014.02.007

[31] Gupta, A., Yunus, M., Sankararamakrishnan, N. "Zerovalent iron encapsulated chitosan nanospheres – A novel adsorbent for the removal of total inorganic Arsenic from aqueous systems", Chemosphere, 86(2), pp. 150–155, 2012.
https://doi.org/10.1016/j.chemosphere.2011.10.003

[32] Awwad, A. M., Salem, N. M. "Kinetics and thermodynamics of Cd(II) biosorption onto loquat (Eriobotrya japonica) leaves", Journal of Saudi Chemical Society, 18(5), pp. 486–493, 2014.
https://doi.org/10.1016/j.jscs.2011.10.007

[33] Zhao, J., Wang, S., Zhang, L., Wang, C., Zhang, B. "Kinetic, Isotherm, and Thermodynamic Studies for Ag(I) Adsorption Using Carboxymethyl Functionalized Poly(glycidyl methacrylate)", Polymers, 10(10), Article number: 1090, 2018.
https://doi.org/10.3390/polym10101090

[34] Guo, H., Stüben, D., Berner, Z. "Removal of arsenic from aqueous solution by natural siderite and hematite", Applied Geochemistry, 22(5), pp. 1039–1051, 2007.
https://doi.org/10.1016/j.apgeochem.2007.01.004